Water Oxidation Hot Paper

DOI: 10.1002/anie.201400243

A Molecular Approach to Self-Supported Cobalt-Substituted ZnO Materials as Remarkably Stable Electrocatalysts for Water Oxidation**

Johannes Pfrommer, Michael Lublow, Anahita Azarpira, Caren Göbel, Marcel Lücke, Alexander Steigert, Martin Pogrzeba, Prashanth W. Menezes, Anna Fischer, Thomas Schedel-Niedrig,* and Matthias Driess**

Dedicated to Professor Schlögl on the occasion of his 60th birthday

Abstract: *In regard to earth-abundant cobalt water oxidation catalysts, very recent findings show the reorganization of the materials to amorphous active phases under catalytic conditions. To further understand this concept, a unique cobalt-substituted crystalline zinc oxide (Co:ZnO) precatalyst has been synthesized by low-temperature solvolysis of molecular heterobimetallic $Co_{4-x}Zn_xO_4$ ($x = 1$–3) precursors in benzylamine. Its electrophoretic deposition onto fluorinated tin oxide electrodes leads after oxidative conditioning to an amorphous self-supported water-oxidation electrocatalyst, which was observed by HR-TEM on FIB lamellas of the EPD layers. The Co-rich hydroxide-oxidic electrocatalyst performs at very low overpotentials (512 mV at pH 7; 330 mV at pH 12), while chronoamperometry shows a stable catalytic current over several hours.*

As fossil fuels decline, future societies will have to rely on sustainable and regenerative energy sources. Ideally this would be hydrogen, as it can be used to store abundant solar energy as a fuel.[1] However, any process using water as a hydrogen source in a (photo)electrochemical cell requires control of the sluggish oxygen evolution reaction (OER), diminishing the overall effectiveness of the water splitting reaction.[2–4] This kinetically hampered four-electron process therefore needs to be mediated by suitable catalysts. Although several materials exist that effectively promote this reaction (for example IrO_2, RuO_2), they usually rely on noble metals. Compounds of earth-abundant cobalt (for example Co_3O_4) have been shown to be suitable catalyst for water oxidation under photo- and electrochemical conditions, be it in a molecular, crystalline, or amorphous state.[5–7] Also substituted cobalt-based perovskites (for example $Ba_{0.5}Sr_{0.5}Co_{0.4}Fe_{0.6}O_{3-\delta}$ and $SrCo_{0.8}Fe_{0.2}O_{3-\delta}$), extended solids, and olivines (such as $LiCoO_2$, $LiCoPO_4$) have been shown active for water oxidation. In this regard, Nocera, Shao-Horn, and co-workers showed that $LiCoO_2$ and $LiCoPO_4$ would transform upon certain anodization conditions into amorphous catalytically active cobalt oxide materials akin to the electrodeposited amorphous cobalt oxide (Co-Pi).[7,8] At basic conditions, a surface amorphization was observed for cobalt-containing perovskites that could be correlated to the activity of the perovskite as a water-oxidation catalyst.[9,10] Surface amorphization or potential-induced transformations also appear to be key features in recently reported highly active manganese oxides.[11,12] In this context, zinc-substituted cobalt based spinels ($ZnCo_2O_4$),[13,14] or cobalt-substituted ZnO structures (Co:ZnO)[15] might be interesting compounds. In both cases, substitution leads to higher p-type conductivity and higher hole density, a priori beneficial properties for the design of supported water oxidation electrocatalysts aimed to be formed in-operando from metastable cobalt-rich oxide precursors.

We aimed at developing a rational bottom-up approach towards intrinsically metastable Co:ZnO nanoparticles as precatalyst for effective (electro)chemical water oxidation. Although CoO dissolves readily in ZnO,[16] high Co concentrations in ZnO demand refined synthetic approaches (including spray pyrolysis and MO-CVD).[17,18] As the solubility of CoO in ZnO changes from bulk to nanoscale and a high surface area is required for catalysis, the preparation of a nanocrystalline Co:ZnO material is imperative.[19] To achieve this, we opted for the solvolysis of suitable CoZn heterobimetallic precursors. As previously shown by Polarz, Driess, and co-workers, heterobimetallic NiZn dipyridyldiol clusters can be thermolyzed ($T_c \geq 250\,^\circ C$) to yield a ZnO phase with a high Ni content.[20] For heterobimetallic molecular Co- and Zn-containing carbamate precursors, the work by Himmel and co-workers shows the formation of Co-substituted ZnO alongside Zn-substituted CoO.[21] To prevent the formation of $ZnCo_2O_4$ spinel phases, a solvothermal

[*] J. Pfrommer, Dr. M. Lublow, Dr. C. Göbel, Dr. P. W. Menezes, Dr. A. Fischer, Prof. Dr. M. Driess
Department of Chemistry, Technische Universität Berlin
Strasse des 17. Juni 135, 10623 Berlin (Germany)
E-mail: anna.fischer@tu-berlin.de
matthias.driess@tu-berlin.de
A. Azarpira, M. Lücke, Dr. A. Steigert, M. Pogrzeba, Dr. T. Schedel-Niedrig
Institut für Solare Brennstoffe
Helmholtz Zentrum für Materialien und Energie
Hahn-Meitner Platz 1, 14109 Berlin (Germany)
E-mail: schedel-niedrig@helmholtz-berlin.de

[**] We thank the BMBF (Light2Hydrogen project, L2H), the Cluster of Excellence UniCat (Exc 314 financed by the DFG and administered by the TU Berlin) and the DFG (SPP1613 project; SolarH2) for financial support. We thank the ZELMI team (TU Berlin) and especially Dr. Dirk Berger and Sören Selve for the FIB preparation and TEM micrographs of the Co:ZnO EPD layers.

Supporting information for this article is available on the WWW under http://dx.doi.org/10.1002/anie.201400243.

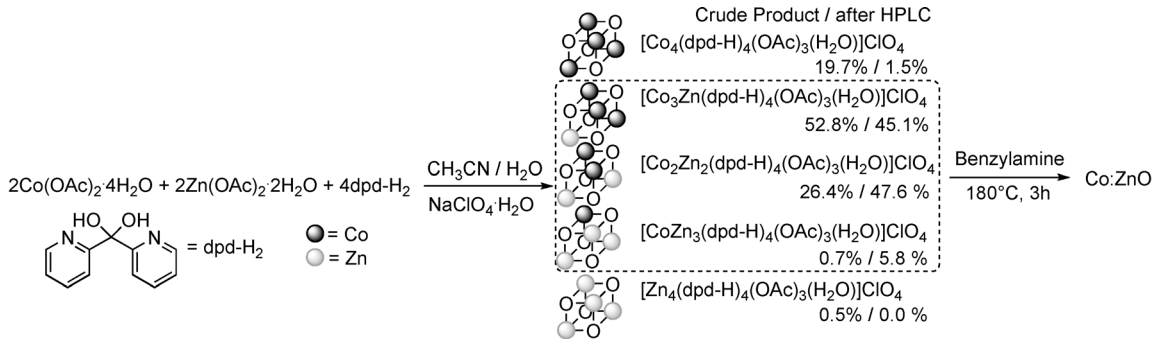

Scheme 1. Synthesis of heterobimetallic $Co_{4-x}Zn_xO_4$ ($x = 1$–3) precursors. Pure homometallic species were obtained if four equivalents of the respective metal acetate were used. Fractions of each species before and after enrichment by HPLC are given next to the formula of the compound. The enriched mixture of heterobimetallic species was solvolyzed to give Co:ZnO.

procedure was developed for the synthesis of Co:ZnO from heterobimetallic dipyridyldiol clusters at low temperatures (180 °C) in benzylamine.[22–24]

For the present work, the synthetic procedures of Polarz, Driess, and co-workers[20] were adapted to produce heterobimetallic CoZn dipyridyldiol clusters. The synthesis yielded a mixture of products containing the homometallic and heterobimetallic compounds (Scheme 1; for the Experimental Section, see the Supporting Information). As anticipated, the entropically favored formation of heterobimetallic species exceeded the amount of homometallic compounds in the crude product.[20] An excess of Co-rich species (owing to decreasing solubility of the clusters with increasing Zn substitution) was evidenced by high-resolution electrospray ionization mass spectrometry (HR ESI-MS; Supporting Information, Figure S1) and inductively coupled plasma optical emission spectroscopy (ICP-OES) in solutions of the crude product (Co 72.1 % : Zn 27.9 %; Supporting Information, Experimental Section). For cluster purification, the crude product was subjected to high-performance liquid chromatography (HPLC). While it was not possible to separate the individual heterobimetallic species, ICP-OES on the yielded solutions (Co 60.5 %, Zn 39.5 %) and signal deconvolution of HR-ESI MS spectra confirmed that the homometallic clusters could be either completely removed (Zn_4dpd-H) or largely separated (Co_4dpd-H) from the product mixture (Scheme 1; Supporting Information, Figure S1 a–d).

The outcome of the solvolysis in benzylamine was dependent on the composition of the precursors. As expected, the solvolysis of the homometallic clusters furnishes brownish-black rock-salt-type CoO and white Wurzite-type ZnO, respectively (Supporting Information, Figure S2). In contrast, the green powder obtained from the solvolysis of HPLC-enriched heterobimetallic precursor solutions could be identified by powder X-ray diffractometry (PXRD) as Wurzite-type ZnO. From the analysis of the lattice parameters (Supporting Information), a Co content of about 30 % could be estimated in the Co:ZnO phase (Supporting Information, Figure S2; Chart S1). ICP-OES on the sample revealed a total amount of 32.4 % Co. Energy-dispersive X-ray spectroscopy (EDX) and high-resolution transmission electron microscopy (HR-TEM) performed on individual particles of the sample confirmed the cobalt incorporation within the ZnO lattice (Supporting Information, Figure S3). This highly Co substituted ZnO phase could only be obtained from the solvolysis of the heterobimetallic precursors, underlining the advantage of using a preorganized molecular architecture (present in the heterobimetallic precursor) to facilitate replacement of lattice metal sites. CoO formation does normally not occur (as evidenced by PXRD). However, depending on the degree of homometallic/heterobimetallic cluster separation, some minor fraction of CoO may form as side product (Supporting Information, Figure S10). In the case where a mixture of the respective homometallic precursors with the same Co to Zn ratio was subjected to solvolysis (same reaction conditions), merely a mixture of CoO and Co:ZnO (denoted as CoO/Co:ZnO) could be obtained. ICP-OES analysis of the latter gave a Co content of 29.4 %. However, analysis of the corresponding PXRDs and respective lattice parameters revealed only marginal Co incorporation within the Co:ZnO phase (Supporting Information, Table S1), as further confirmed by TEM and EDX analysis (Supporting Information, Figure S2 d, Figure S3–1/2). Finally, elemental analysis (EA) of all samples showed only traces of carbon in the samples (< 1 %), ruling out the possibility that excess Co is found in remnants of the metal-organic precursors.

To evaluate the potential of the as prepared Co:ZnO particles as water oxidation catalyst, the samples were subjected to the $(NH_4)_2Ce(NO_3)_6$ (cerium ammonium nitrate, CAN) model reaction.[25] The evolution of molecular oxygen was monitored with a Clark-type oxygen electrode (Supporting Information, Figure S4). Remarkably, CoO (solvolysis of homometallic Co precursor) and in particular Co:ZnO (solvolysis of heterobimetallic Co-Zn precursor) show unusually high rates for oxygen evolution, while the phase-segregated CoO/Co:ZnO composite material (solvolysis of a mixture of homometallic precursors) as well as commercial CoO (Aldrich, > 100 nm) and Co_3O_4 (Aldrich, > 50 nm) nanopowders (Table 1) were only marginally active. After the reaction, all solvolytically prepared samples became black. TEM investigation after the CAN reaction of the most active Co:ZnO sample showed an important loss of crystallinity. Furthermore, partially amorphous sheets could be observed, containing Co and Zn (Supporting Information, Figure S3-3; Table S2). These results were in good agreement with some of

Table 1: Summary of the physical parameters of the samples.

Sample	Mean CS [nm][a]	[%] Co[b]	S_{BET} [$m^2 g^{-1}$][c]	n_{O_2} mol Co^{-1} [mmol s^{-1}][d]
CoO (commercial)	72	–	25.5	0.03
Co_3O_4 (commercial)	41	–	49.4	0.15
CoO	15	–	75.9	4.77
Co:ZnO/CoO	33	32.4	33.1	0.04
Co:ZnO	43	29.4	35.5	28.23

[a] Mean crystallite size (CS) as determined by the Debye–Scherrer equation. [b] As determined by ICP-OES. [c] As determined by BET. [d] As determined from the first 20 seconds of Clark electrode measurements on Ce^{IV} treated sample suspensions in water.

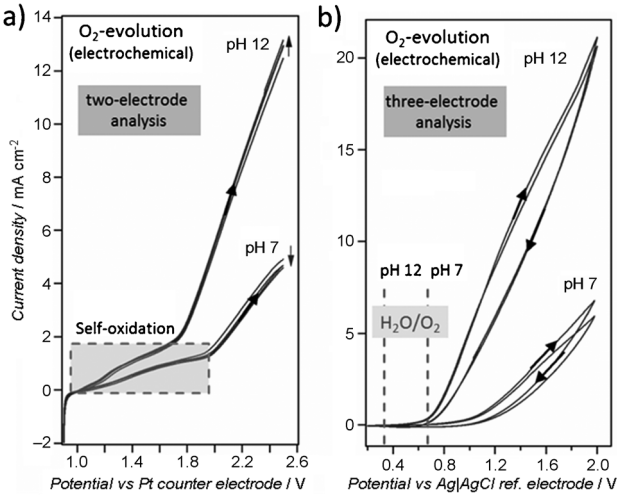

Figure 1. a) Two-electrode current–potential plot showing self-oxidation of the film during the forward scan; b) three-electrode current–voltage plot featuring less-prominent oxidation peaks. The measurements were conducted in a 0.1 M KPi electrolyte at pH 7 (a) and pH 12 (b) with a scan rate of 20 mV s^{-1}.

our recent findings indicating that MnO particles fabricated from benzylamine are prone to surface oxidation under oxidizing conditions, forming an highly active amorphous water oxidation catalyst.[26]

In terms of particle size and surface area solvolytically prepared CoO nanopowders deviates most from all the samples, featuring the smallest particle size (15 nm) and the highest surface area (75.2 $cm^2 g^{-1}$); both explaining the high activity compared to commercial CoO and phase-segregated CoO/Co:ZnO. The highest activity observed for Co:ZnO cannot be explained by a size effect, but rather relates to the high substitution of cobalt within the ZnO lattice. Indeed comparison of the activity of CoO/Co:ZnO powders with lowly Co-substituted Co:ZnO with the activity of highly substituted Co:ZnO powders of similar particle size and surface area (see Table 1), indicates that the degree of cobalt substitution within the Co:ZnO lattice must be a decisive factor for the increased OER activity of the metastable Co:ZnO particles (Supporting Information, Figure S4).

For analysis of the electrocatalytic properties of the as prepared Co:ZnO material (in KPi electrolytes), the powders were deposited onto fluoride-doped tin oxide substrates (FTO). The deposition was performed by electrophoretic deposition (EPD) from powder dispersions in acetone/iodine mixtures (for experimental details, see the Supporting Information). Grazing incident X-ray diffraction (GIXRD; Supporting Information, Figure S5) and scanning electron microscopy (SEM; Supporting Information, Figure S6) confirmed the formation of relatively homogeneous Co:ZnO films fully covering the FTO substrate and build out of loosely packed particles. Subsequent analysis of the current density behavior coupled with in situ differential electrochemical mass spectroscopy (DEMS) for molecular oxygen detection revealed that the as prepared Co:ZnO electrodes exhibit low overpotential (330 mV, pH 12; 590 mV, pH 7) and high stability for oxygen evolution in potassium phosphate (KPi) or Na_2SO_4 electrolytes at neutral and alkaline pH (pH 7 and pH 12, respectively; Figure 1; Supporting Information, Figures S7, S8). Beside oxygen evolution, self-oxidation of the as-prepared films, attributed to the oxidation of $Co^{II} \rightarrow Co^{III}$, was observed at lower potentials during cyclovoltammetry (CV), leading to higher oxidation states of the ternary composite. If the Co:ZnO loading of the electrode is very low (< 1 mg), only the first cycle shows this self-oxidation peak. As previously observed (CAN test), the color of the Co:ZnO film changed irreversibly from green to black along with the formation of an amorphous over-coating on the electrode surface (see HRSEM images in the Supporting Information, Figure S6).

At basic pH, water can be oxidized over several hours at a potential of 0.8 V vs. Ag/AgCl without any decrease in current density (Supporting Information, Figure S9). The latter exemplifies the high stability of the working catalyst. When comparing cyclovoltammetry data of thin EPD layers of Co:ZnO with the Co oxide catalysts from the CAN experiments (Supporting Information, Figure S10), a different electrochemical behavior can be seen for all four catalysts: solvolytically prepared CoO particles show the earliest response to the applied potential, however Co:ZnO facilitates higher catalytic currents as the potential increases.

TEM analysis of a FIB lamella of the Co:ZnO EPD layer before and after electrocatalysis (EC) shows, in agreement with the GI-XRD measurements (Supporting Information, Figure S5), that the deposited Co:ZnO film after EC is composed of small Co:ZnO particles and a few very large (ca. 1 μm) CoO particles. Close examination of the small Co:ZnO particles with HR-TEM revealed, in agreement with the HR-SEM data, the formation of an amorphous hull around the crystallites that was not present at the as-prepared Co:ZnO after the EPD process (Figure 2a; Supporting Information, Figure S11). EDX analysis of the small Co:ZnO particles shows that they still contain large amounts of Co (Supporting Information, Chart S2, Figure S12), although some Co leaching was observed.

EDX investigation of the electrode after EC (Supporting Information, Figure S6) and surface-sensitive X-ray photoelectron spectroscopy (XPS; pH 7, 0.8 V) revealed that the amorphous, newly deposited layer contains both Co and Zn (Supporting Information, Figure S13). The main intensive broad $Co2p_{3/2}$ core level (FWHM of (3.3 ± 0.1) eV) occurs at (780.8 ± 0.1) eV, accompanied by so-called satellite features

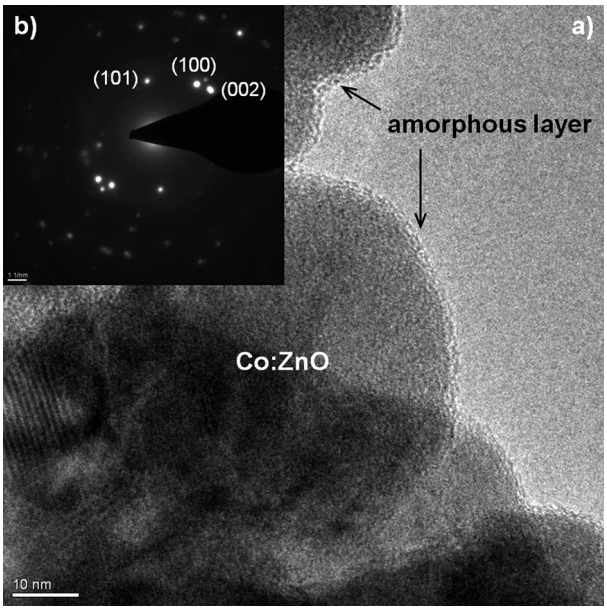

Figure 2. a) HR-TEM micrograph of a FIB-layer of Co:ZnO particles after electrocatalysis in 0.1 M KPi at pH 12 featuring a thin amorphous surface layer. Scale bar: 10 nm. b) Respective selected area electron diffraction (SAED) pattern of the particles indexed according to the Wurzite-type ZnO structure. Scale bar: 1 nm^{-1}.

at higher binding energies (BEs) ranging up to about 793 eV.[27] Compared to recently published data of cobalt oxides and cobalt hydroxides, we assign the Co $2p_{3/2}$ core level to mixed Co^{II} and Co^{III} oxidation states. The best spectral agreement is achieved with the reference spectrum of the cobalt hydroxide phase, $Co(OH)_2$, that is, Co^{II}, BE of 780.7 eV, with some contributions of Co^{III}, most likely due to the presence of CoOOH.[28,29] The corresponding O 1s core-level spectrum (Supporting Information, Figure S13) confirms the presence of a dominating cobalt(II) hydroxide surface phase with a characteristic BE at (531.0 ± 0.1) eV. A quantification of the amount of Co and Zn surface atoms in the catalytically active over-layer from the XPS data was obtained by taking into account the atomic subshell photoionization cross sections and asymmetry parameters,[30] showing a Co:Zn ratio of 1:0.134, although an unknown fraction of the Zn signals originate from the underlying Co:ZnO precatalyst. As the Co:Zn ratio observed by EDX in the amorphous sheets formed in the Co:ZnO sample after CAN treatment is similar (Supporting Information, Table S2 and Figure S3-3), a similar catalytically active species was likely present in both experiments. Further XPS analysis of Co:ZnO electrodes at different potentials and pH is currently underway.

In the context of recent results, we highlight Co^{II}-loaded FTO substrates (Co@FTO), which upon anodization form a Co^{III}-containing small molecule assembly as a water oxidation catalyst,[31] and show similar reactivity. However, we exclude this active species in the case described herein as we observed at anodized electrode hydroxy-oxidic surface features (Supporting Information, Figure S9). This leads to the conclusion that the formation of the amorphous CoZn water oxidation catalyst is a product of the superficial oxidation of the metastable Co^{II}-rich Co:ZnO precatalyst, forming a hydroxyoxylated film.[32] CoOOH species are layered structures which have been shown to be the active species in water-oxidation catalysts such as Co_3O_4[33,34] and are closely related to the CoZn layered double hydroxide (LDH) described by Zou et al., who showed the beneficial influence of Zn in LDH for electrochemical water oxidation, where the redox-inert Zn^{II} ion appears to provide structural guidance to the catalytically active Co species.[35] From the Pourbaix diagram of Chivot et al., it could be determined that a CoOOH phase should be stable at the applied pH and potential.[36] The influence of the Co:ZnO support is currently examined by conductivity measurments on pristine and oxidized phases.

In summary, we have presented a novel and effective way to prepare a very stable heterobimetallic catalyst for water oxidation by a rational molecular approach. The Co:ZnO material shows considerably low overpotential and consists of an amorphous hydroxyoxylated CoZn overlayer formed in situ and self-supported on crystalline Co:ZnO particles. The active $Co^{II/III}$-containing layer originates directly from the metastable and highly cobalt-substituted ZnO particles. As a result, the amorphous water oxidation catalyst overlayer and the crystalline Co:ZnO support are remarkably well-integrated. The successful rational approach to self-supported cobalt substituted ZnO materials described herein, taking advantage of the inorganic core architecture of CoZn heterobimetallic precursors, is a powerful method which could be extended to the low temperature synthesis of other desired very stable heterobimetallic water oxidation catalyst based on earth-abundant metals.

Received: January 9, 2014
Published online: April 28, 2014

Keywords: amorphous materials · electrocatalysis · heterogeneous catalysis · self-activation · water oxidation

[1] J. O. M. Bockris, *Int. J. Hydrogen Energy* **2002**, *27*, 731.
[2] H. Dau, C. Limberg, T. Reier, M. Risch, S. Roggan, P. Strasser, *ChemCatChem* **2010**, *2*, 724.
[3] H. Dau, I. Zaharieva, *Acc. Chem. Res.* **2009**, *42*, 1861.
[4] H. Inoue, T. Shimada, Y. Kou, Y. Nabetani, D. Masui, S. Takagi, H. Tachibana, *ChemSusChem* **2011**, *4*, 173.
[5] M. Grzelczak, J. Zhang, J. Pfrommer, J. Hartmann, M. Driess, M. Antonietti, X. Wang, *ACS Catal.* **2013**, *3*, 383.
[6] V. Artero, M. Chavarot-Kerlidou, M. Fontecave, *Angew. Chem.* **2011**, *123*, 7376; *Angew. Chem. Int. Ed.* **2011**, *50*, 7238.
[7] M. W. Kanan, D. G. Nocera, *Science* **2008**, *321*, 1072.
[8] S. W. Lee, C. Carlton, M. Risch, Y. Surendranath, S. Chen, S. Furutsuki, A. Yamada, D. G. Nocera, Y. Shao-Horn, *J. Am. Chem. Soc.* **2012**, *134*, 16959.
[9] K. J. May, C. E. Carlton, K. A. Stoerzinger, M. Risch, J. Suntivich, Y.-L. Lee, A. Grimaud, Y. Shao-Horn, *J. Phys. Chem. Lett.* **2012**, *3*, 3264.
[10] M. Risch, A. Grimaud, K. J. May, K. A. Stoerzinger, T. J. Chen, A. N. Mansour, Y. Shao-Horn, *J. Phys. Chem. C* **2013**, *117*, 8628.
[11] M. Fekete, R. K. Hocking, S. L. Y. Chang, C. Italiano, A. F. Patti, F. Arena, L. Spiccia, *Energy Environ. Sci.* **2013**, *6*, 2222.

[12] S. L. Y. Chang, A. Singh, R. K. Hocking, C. Dwyer, L. Spiccia, *J. Mater. Chem. A* **2014**, *2*, 3730.
[13] A. Zakutayev, T. R. Paudel, P. F. Ndione, J. D. Perkins, S. Lany, A. Zunger, D. S. Ginley, *Phys. Rev. B* **2012**, *85*, 085204.
[14] B. Chi, J. Li, X. Yang, H. Lin, N. Wang, *Electrochim. Acta* **2005**, *50*, 2059.
[15] A. C. Tuan, J. D. Bryan, A. B. Pakhomov, V. Shutthanandan, S. Thevuthasan, D. E. McCready, D. Gaspar, M. H. Engelhard, J. W. Rogers, Jr., K. Krishnan, D. R. Gamelin, S. A. Chambers, *Phys. Rev. B* **2004**, *70*, 054424.
[16] N. H. Perry, T. O. Mason, *J. Am. Ceram. Soc.* **2013**, *96*, 966.
[17] V. Jayaram, J. Rajkumar, B. S. Rani, *J. Am. Ceram. Soc.* **1999**, *82*, 473.
[18] R. Djenadic, G. Akgül, K. Attenkofer, M. Winterer, *J. Phys. Chem. C* **2010**, *114*, 9207.
[19] C. Ma, A. Navrotsky, *Chem. Mater.* **2012**, *24*, 2311.
[20] S. Polarz, A. V. Orlov, M. W. E. van den Berg, M. Driess, *Angew. Chem.* **2005**, *117*, 8104; *Angew. Chem. Int. Ed.* **2005**, *44*, 7892.
[21] D. Domide, O. Walter, S. Behrens, E. Kaifer, H.-J. Himmel, *Eur. J. Inorg. Chem.* **2011**, 860.
[22] M. Niederberger, *Acc. Chem. Res.* **2007**, *40*, 793.
[23] M. Niederberger, G. Garnweitner, *Chem. Eur. J.* **2006**, *12*, 7282.
[24] M. Niederberger, G. Garnweitner, N. Pinna, G. Neri, *Prog. Solid State Chem.* **2005**, *33*, 59.
[25] J. Kiwi, M. Gratzel, G. Blondeel, *J. Chem. Soc. Dalton Trans.* **1983**, 2215.
[26] A. Indra, P. W. Menezes, I. Zaharieva, E. Baktash, J. Pfrommer, M. Schwarze, H. Dau, M. Driess, *Angew. Chem.* **2013**, *125*, 13447; *Angew. Chem. Int. Ed.* **2013**, *52*, 13206.
[27] N. S. McIntyre, M. G. Cook, *Anal. Chem.* **1975**, *47*, 2208.
[28] J. Yang, H. Liu, W. N. Martens, R. L. Frost, *J. Phys. Chem. C* **2010**, *114*, 111.
[29] M. C. Biesinger, B. P. Payne, A. P. Grosvenor, L. W. M. Lau, A. R. Gerson, R. S. C. Smart, *Appl. Surf. Sci.* **2011**, *257*, 2717.
[30] J. J. Yeh, I. Lindau, *At. Data Nucl. Data Tables* **1985**, *32*, 1.
[31] C. A. Kent, J. J. Concepcion, C. J. Dares, D. A. Torelli, A. J. Rieth, A. S. Miller, P. G. Hoertz, T. J. Meyer, *J. Am. Chem. Soc.* **2013**, *135*, 8432.
[32] Y. Surendranath, D. A. Lutterman, Y. Liu, D. G. Nocera, *J. Am. Chem. Soc.* **2012**, *134*, 6326.
[33] M. Bajdich, M. García-Mota, A. Vojvodic, J. K. Nørskov, A. T. Bell, *J. Am. Chem. Soc.* **2013**, *135*, 13521.
[34] M. García-Mota, M. Bajdich, V. Viswanathan, A. Vojvodic, A. T. Bell, J. K. Norskov, *J. Phys. Chem. C* **2012**, *116*, 21077.
[35] X. Zou, A. Goswami, T. Asefa, *J. Am. Chem. Soc.* **2013**, *135*, 17242.
[36] J. Chivot, L. Mendoza, C. Mansour, T. Pauporté, M. Cassir, *Corros. Sci.* **2008**, *50*, 62.

